Pergamon

Bioorganic & Medicinal Chemistry 10 (2002) 3415–3423

BIOORGANIC & MEDICINAL CHEMISTRY

1,4-Benzothiazine and 1,4-Benzoxazine Imidazole Derivatives with Antifungal Activity: A Docking Study

Antonio Macchiarulo,[a] Gabriele Costantino,[a] Daniele Fringuelli,[b] Anna Vecchiarelli,[c] Fausto Schiaffella[a] and Renata Fringuelli[a,*]

[a]*Department of Drug Chemistry and Technology, Via del Liceo 1, University of Perugia, 06123 Perugia, Italy*
[b]*Applied and Clinical Biochemistry Section, Department of Internal Medicine, Via del Giochetto, University of Perugia, 06122 Perugia, Italy*
[c]*Microbiology Section, Department of Experimental Medicine and Biochemical Sciences, Via del Giochetto, University of Perugia, 06122 Perugia, Italy*

Received 16 April 2002; accepted 28 June 2002

Abstract—We have recently described the synthesis and antifungal activity of a series of 1,4-benzothiazine and 1,4-benzoxazine imidazole derivatives that mainly showed in vivo activity against a murine experimental model of candidiasis but that very often lacked in vitro activity. Here, we report a docking study of a representative set of our molecules in a 3D model of CYP51 of *Candida albicans* (CA-CYP51). The model was constructed on the basis of the sequence homology relationship with the recently reported crystal structure of the CYP51 of *Mycobacterium tuberculosis* (MT- CYP51).

Introduction

During the past two decades, the frequency of invasive and systemic fungal infections has increased dramatically in the population with altered immunity.[1,2]

Current available therapy in treating fungal infections can suffer from drug related toxicity, hazardous drug–drug interactions, non-optimal pharmacokinetics and development of drug resistance. [3]

Azoles are currently the most widely studied class of antifungal agents,[4] and fluconazole is the agent of choice for *Candida* infections. Enzymes in the ergosterol-biosynthesis pathway, specifically the cytochrome P450-dependent lanosterol 14α-demethylase ($P450_{14DM}$, CYP51), are the targets for successfully marketed antifungal drugs.

Azoles inhibit CYP51 causing accumulation of methylated sterols, depletion of ergosterol, and inhibition of cell growth.[5]

We have recently described the synthesis and antifungal activity of a series of 1,4-benzothiazine and 1,4-benzoxazine imidazole derivatives that mainly showed in vivo activity against a murine experimental model of candidiasis but that very often lacked in vitro activity.[6–9]

As part of our research project, we studied how our molecules may be interacting at the target enzyme. Indeed, the understanding of the molecular basis of such interaction should help in the design of more active inhibitors. Here, we report a docking study of a set of our azole inhibitors (Chart 1) in a 3D model of CYP51 of *Candida albicans* (CA-CYP51). The model was constructed on the basis of the sequence homology relationship with the recently reported crystal structure of the CYP51 of *Mycobacterium tuberculosis* (MT-CYP51, pdb code: 1ea1, 1e9x).[10]

Results

Homology modeling

The alignment of sequences of CA-CYP51 and those of the crystal structures of MT-CYP51 in complex with fluconazole and 4-phenylimidazole are shown in Figure

*Corresponding author. Tel.: +39-075-585-5134; fax: +39-075-585-5161; e-mail: fringuel@unipg.it

0968-0896/02/$ - see front matter
PII: S0968-0896(02)00263-8

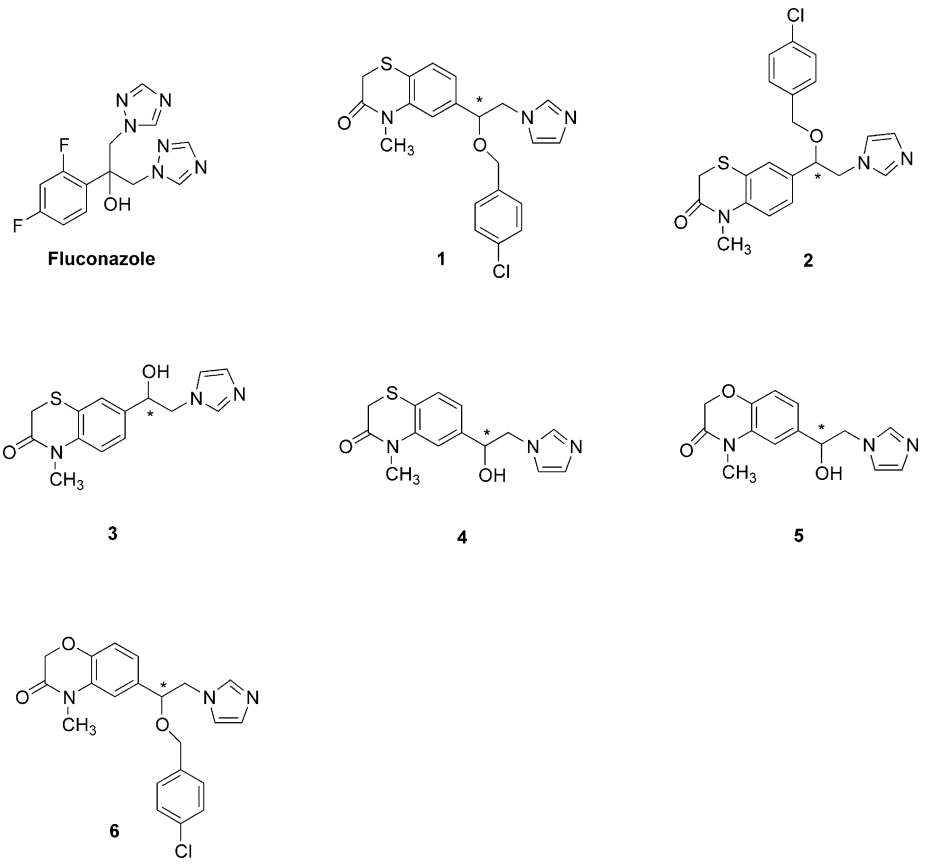

Chart 1.

1. CA-CYP51 and MT-CYP51 share a sequence homology of 40% with 22% identical residues.

The Verify-3D plots of MT-CYP51 structures and of the 3-D model of CA-CYP51 are reported in Figure 2 indicating the statistical accuracy of the proposed fold for CA-CYP51.

The model of CA-CYP51 was superimposed on the crystal structures of MT-CYP51 by fitting all the heavy atoms along the backbone, on the basis of the proposed alignment. The average RMS deviation was 1.01 Å. The largest deviation occurred in the amino terminal region comprising residues from Cys134 to Phe145. The overall topography of the enzyme is very similar to that of MT-CYP51 and is described elsewhere.[10] Two large insertions (>5 residues) were present in the CA-CYP51 model and designated as loops. They correspond to residues from Glu174 to Thr182 and from Thr429 to Phe449. These insertions are located on the surface of the model and exposed to the solvent. Other small insertions and deletions were present in CA-CYP51 but they did not cause perturbations in the folding of the enzyme in comparison to that of MT-CYP51 (Fig. 3).

The enzyme bound the heme group through a set of conserved and not conserved residues relative to the crystal structures of MT-CYP51 (Fig. 1). Conserved residues comprised Tyr118, Thr311, Pro375, Arg381, Phe463, His468, Cys470, Gly472, Phe475 and Ala476. The not conserved residues were Lys143 and Gly307. The active site of CA-CYP51 was defined by the heme group and by those residues aligned to positions belonging to a sphere of radius 10 Å centered on fluconazole in the crystallized complex of MT-CYP51.

Docking of inhibitors

A knowledge-based strategy was used to perform docking experiments of fluconazole and of a set of 1,4-benzothiazine and 1,4-benzoxazine imidazole derivatives (Chart 1) into the catalytic site of CA-CYP51. Although the binding site of azole inhibitors in the crystal of MT-CYP51 is filled by water molecules which mediate the interactions between ligands and enzymes, they were not considered during docking experiments because of the impossibility of predicting possible rearrangements of their positions upon binding of structurally diverse inhibitors. Where present, both the *R* and *S* isomers of compounds were considered for docking experiments. Fluconazole binds to the active site of CA-CYP51 through the formation of a coordination bond with the iron of heme group and several *non*-bonded interactions involving a cluster of hydrophobic residues (Tyr118, Leu121, Phe228, Gly307, Thr311, Leu376, Met508). The docked conformation of fluconazole into the binding site of CA-CYP51 was similar to the bioactive conformation of fluconazole into the crystallized complex of MT-CYP51 (Fig. 4).

Both the *R* and *S* isomers of **1** interact with CA-CYP51 through a similar pattern of interaction but using different

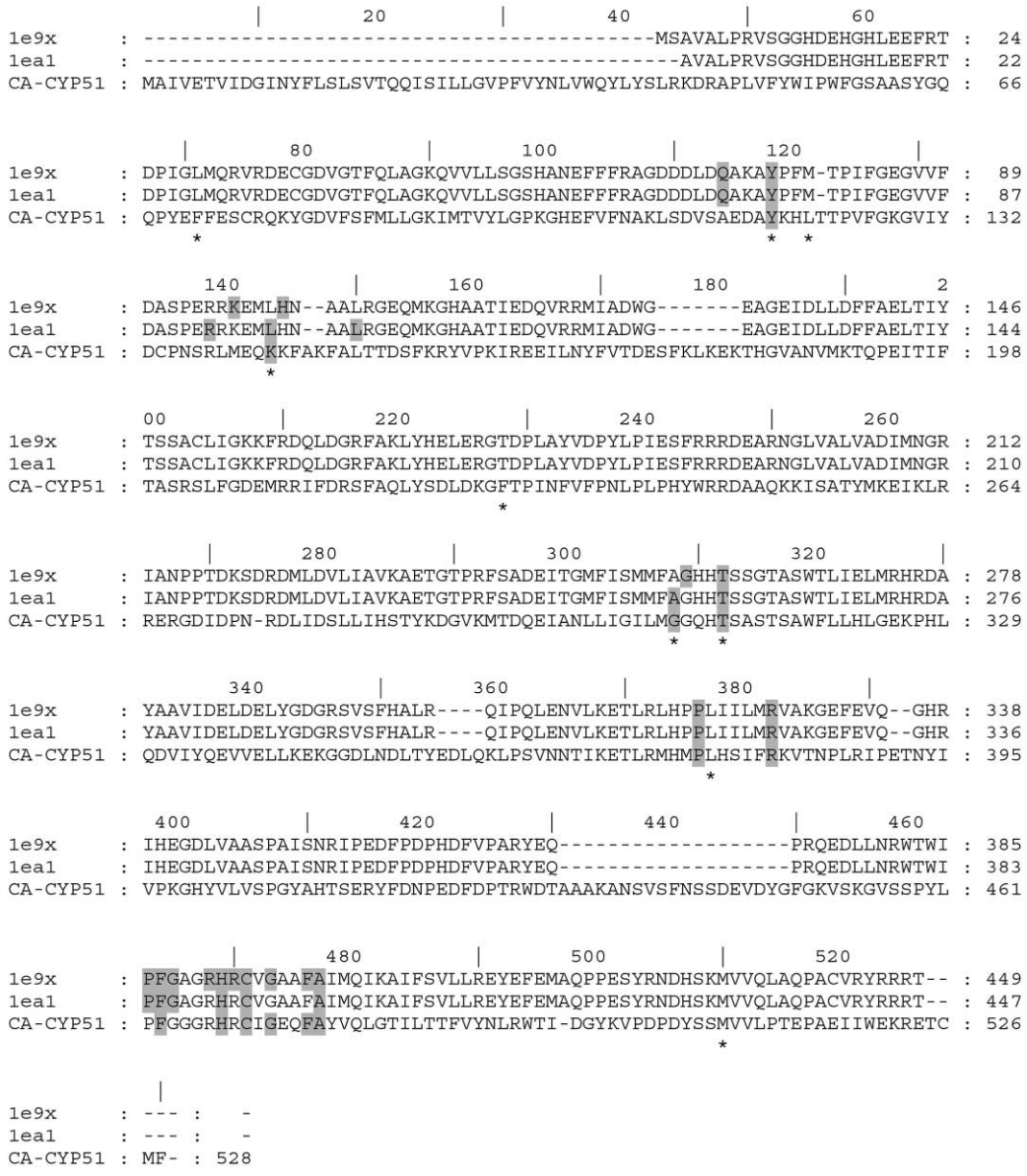

Figure 1. Alignment of sequences of CA-CYP51 and MT-CYP51 (1e9x, 1ea1). Residues involved in binding of heme group are gray shaded. Residues involved in the binding of azole inhibitors in the catalytic site are marked by a star.

conformations. Besides the coordination bond of the imidazole ring with the iron of the heme group, non-bonded interactions involve the benzothiazine moiety of **1** and hydrophobic residues such as Phe71 and Leu121. The *p*-chlorophenyl group interacts with the side chain of Tyr118 through the formation of a π–π face-to-edge interaction and with hydrophobic residues (Phe228, Leu376, Met508) through *non*-bonded interactions (Fig. 5). An aromatic-cation interaction involves the π electrons of the benzene group of the benzothiazine moiety and the positively charged Lys143.

The *R* and *S* forms of compound **2** interact with CA-CYP51 through the formation of a coordination bond between the imidazole ring and the heme group. Several non-bonded interactions stabilize the coordination bond and involve Leu121, Phe71, Lys143, Phe228, Leu376 and Met508. The presence of intra-molecular and inter-molecular π–π interactions involving the *p*-chlorophenyl group, the benzothiazine moiety, and the aromatic ring of Tyr118 enforces the binding of the *S* over the *R* isomer of **2** (Fig. 5).

Compounds **3** (Fig. 5) and **4** (Fig. 6) adopt a similar binding mode into the active site of the enzyme. Their benzothiazine moiety interacts with a cluster of hydrophobic residues (Phe71 and Leu121) while the imidazole ring makes a coordinative bond with the iron of the heme group. No direct interaction is observed for their free hydroxyl group.

Compound **5** adopts a similar interaction pattern as described above for compounds **3** and **4**. It is noteworthy that the ether oxygen of the benzoxazine group interacts with Lys143 through the formation of an hydrogen bond (Fig. 6).

A binding conformation similar to that of compound **1** can also be reported for compound **6**. Briefly, compound

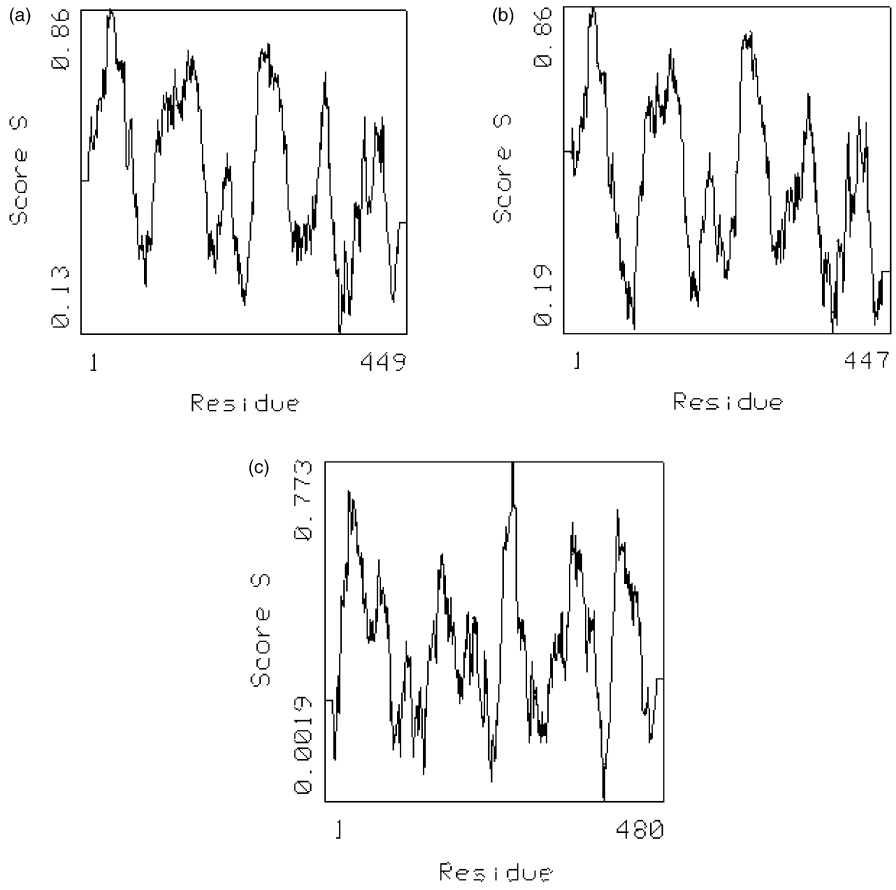

Figure 2. Verify-3D plots of the crystal structures of MT-CYP51 (a, 1e9x; b, 1ea1) and of the 3D model of CA-CYP51 (c).

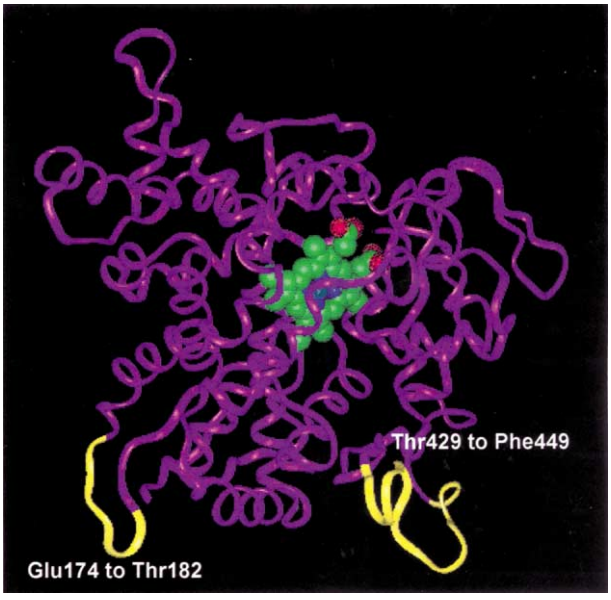

Figure 3. Structure and topology of CA-CYP51. The two large loop insertions are highlighted in yellow. The structure of heme group is in CPK.

6 coordinates the sixth position of the iron of the heme group with the nitrogen in position 3 of its imidazole ring. This interaction is stabilized by non-bonded contacts involving the benzoxazine group and a cluster of residues comprising Phe71 and Leu121. An aromatic–cation interaction is formed between the benzene ring of the benzoxazine group and the side chain of Lys143. Again, the *p*-chlorophenyl group of **6** interacts with the side chain of Tyr118 through the formation of a π–π face-to-edge stacking and forms hydrophobic interactions with Phe228, Leu376, and Met508 (Fig. 6).

Discussion

Cytochrome P450 14α-sterol demethylases (CYP51s) constitute a family of enzymes which catalyze the oxidative removal of the 14α-methyl group of lanosterol derivatives in yeast, fungi, plants and mammalian cells. On the basis of the sequence homology between MT-CYP51 and CA-CYP51, a 3D model of CYP51 of *C. albicans* was built and exploited to study the interactions between a set of benzothiazine and benzoxazine imidazole derivatives and its catalytic site. The antifungal activity of these compounds is expressed as their in vitro minimum inhibitory concentrations (MIC values, Table 1). It should be mentioned that this value of activity is not the best choice for a structure–activity relationship (SAR) study. Indeed, besides the inhibition of the enzyme, other factors coupled to the drug adsorption phase through the membrane of the fungi can affect the MIC values. Nevertheless, the lack of an enzymatic assay for these compounds prompted us to use the MIC values and to introduce the logP value as a parameter describing the drug adsorption phase.

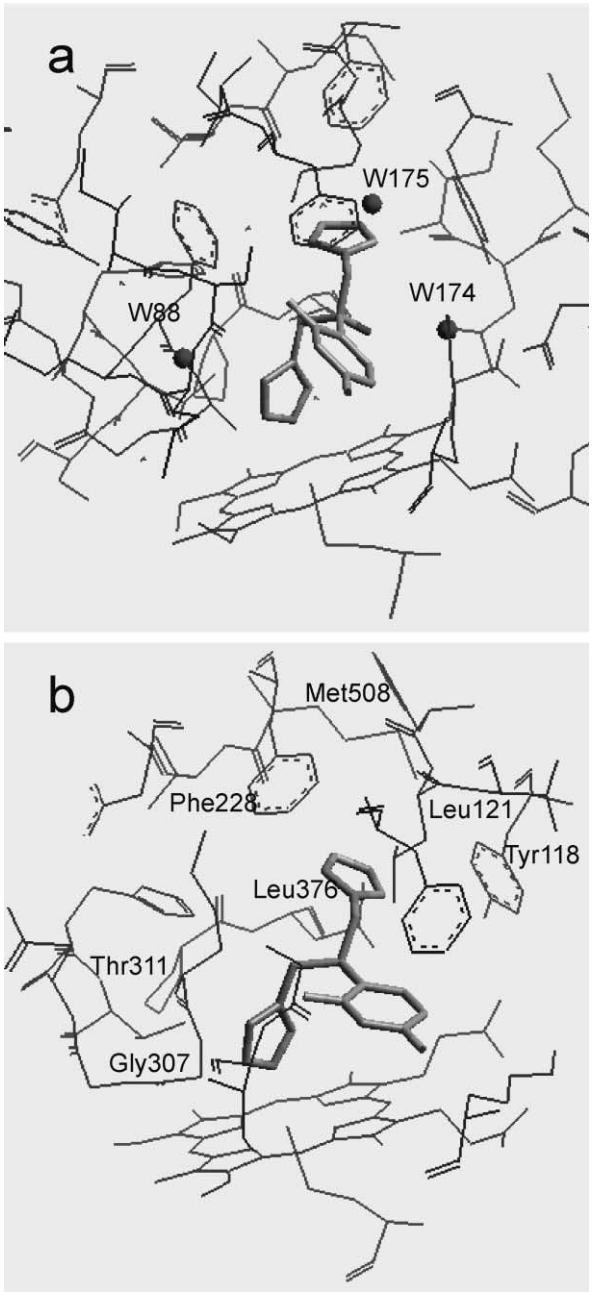

Figure 4. (a) Binding mode of fluconazole into the catalytic site of MT-CYP51 (pdb code: 1ea1). Water molecules interacting with the inhibitor are represented in balls; (b) Best docking solution of fluconazole into the catalytic site of CA-CYP51.

Docking experiments report a similar binding mode for fluconazole and the set of studied compounds. In particular, fluconazole binds to the catalytic site of CA-CYP51 adopting a similar bio-active conformation as observed in its crystallized complex with MT-CYP51 (pdb code: 1ea1).

Thus, mutations in CA-CYP51 catalytic sites, such as L143K and T228F, do not affect the binding mode of fluconazole. In particular, the positively charged side chain of Lys143 does not interact with fluconazole. Indeed, it points towards a carboxylic moiety of the heme group. The residue of phenylalanine (T228F substitution) belongs to a cluster of hydrophobic residues in the catalytic site of CA-CYP51 which interact with fluconazole.

To analyze docking solutions in terms of structure–activity relationship, as discussed above both the binding energies and the logP (expressed as AlogP)[11] were evaluated for each compound. The results are summarized in Table 1.

Fluconazole and compound **6** are the most active compounds among those studied. Nevertheless their binding energies, respectively −29.10 kcal/mol and −30.813 kcal/mol (*S* isomer), do not score them as the most active molecules. This contradiction could be explained by the role of water in affecting the binding of the inhibitors to the enzyme. Indeed, it is worth noting that in the complex with MT-CYP51, fluconazole interacts with at least three water molecules which make bridge interactions with the catalytic site of the enzyme. Moreover, several other water molecules fill the catalytic site of MT-CYP51. As a consequence, structural water could play a pivotal role in enforcing the binding of fluconazole and other inhibitors to the enzyme. The fact of not considering structural water as part of CA-CYP51 could lead to an underestimation of the binding energies of fluconazole and **6**. In this light, the replacement of the ether oxygen of the benzoxazine moiety (compound **6**) with the sulfur atom in structures **1** and **2** could be overestimated in terms of binding energies since our model does not take into account the loss of possible hydrogen bonds between the ether oxygen and the enzyme mediated by the water.

Compound **2** (*S* isomer: −40.142 kcal/mol) is scored better than **1** (*S* isomer: −31.804 kcal/mol) as expected from the MIC activities of these inhibitors. Both compounds prefer the *S* isomer over the *R* form. The orientation adopted by the benzothiazine moiety of compound **2** in the catalytic site of CA-CYP51 is different from that of **1** and from the benzoxazine group of compound **6**. Thus, the improvement of MIC and binding energy observed for **2** compared to **1** could be ascribed to the change of the side chain to position 7 of the benzothiazine nucleus. In particular, this substitution promotes a π–π stacking interaction between the benzothiazine moiety and the *p*-chlorophenyl group of the molecule in the bioactive conformation of this compound. This aromatic intra-molecular interaction reinforces the inter-molecular π–π interaction involving the *p*-chlorophenyl group and the aromatic side chain of Tyr61.

The discrepancy between the MIC values of **3, 4** and **5** and their respective binding energies should be ascribed to the high hydrophilic character of these compounds (**3**-AlogP = 0.50, **4**-AlogP = 0.50, **5**-AlogP = 0.16). Indeed, although **3**, **4** and **5** fit well the catalytic site of the enzyme, an higher logP value is required to cross the membrane of fungi and reach the enzyme.

For all compounds of the series the *S* isomers fit the catalytic site of the enzyme better than the *R* forms, with only one exception. In compound **3** the change of

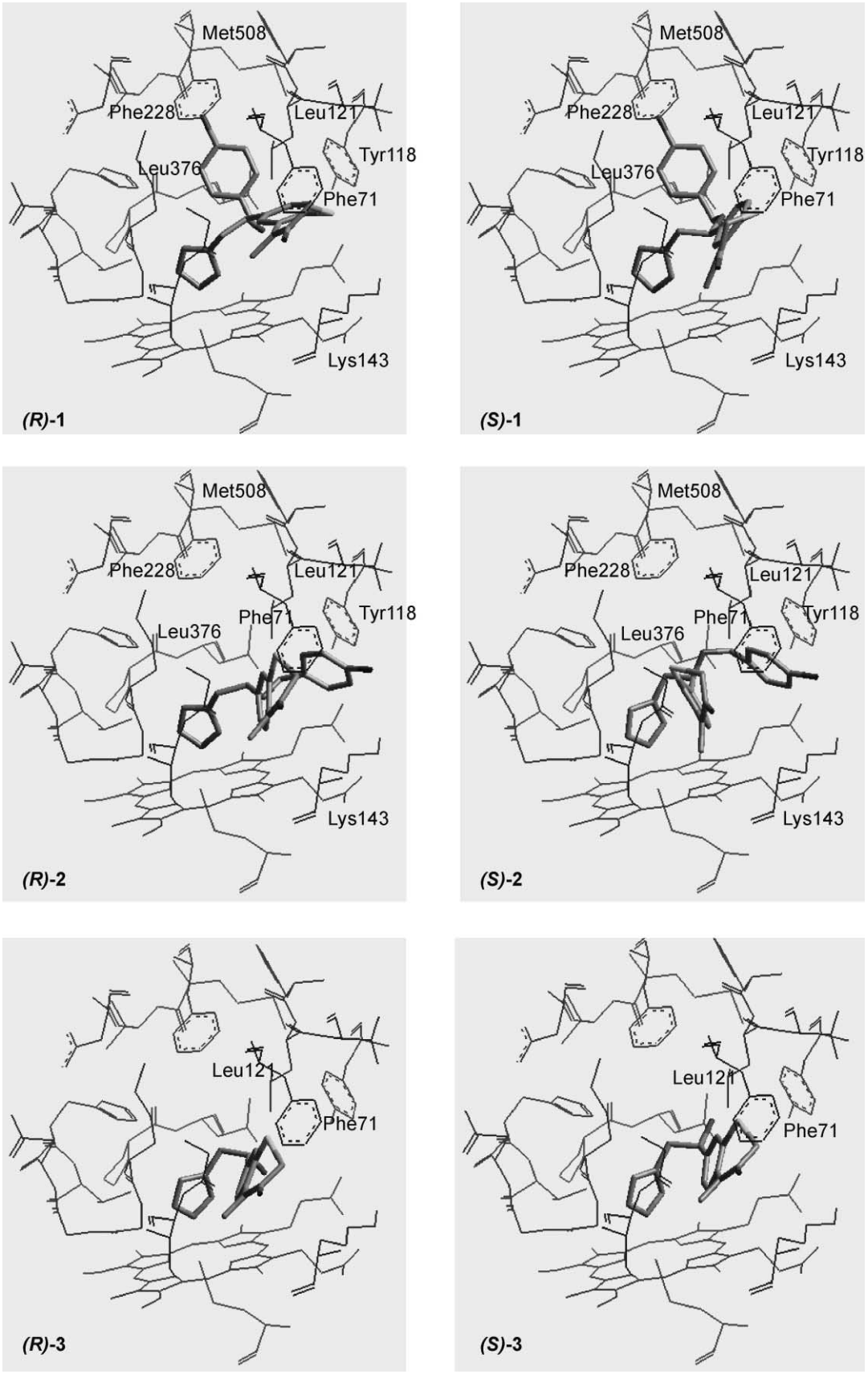

Figure 5. Docking solutions of the isomers of compounds **1**–**3** into the catalytic site of CA-CYP51.

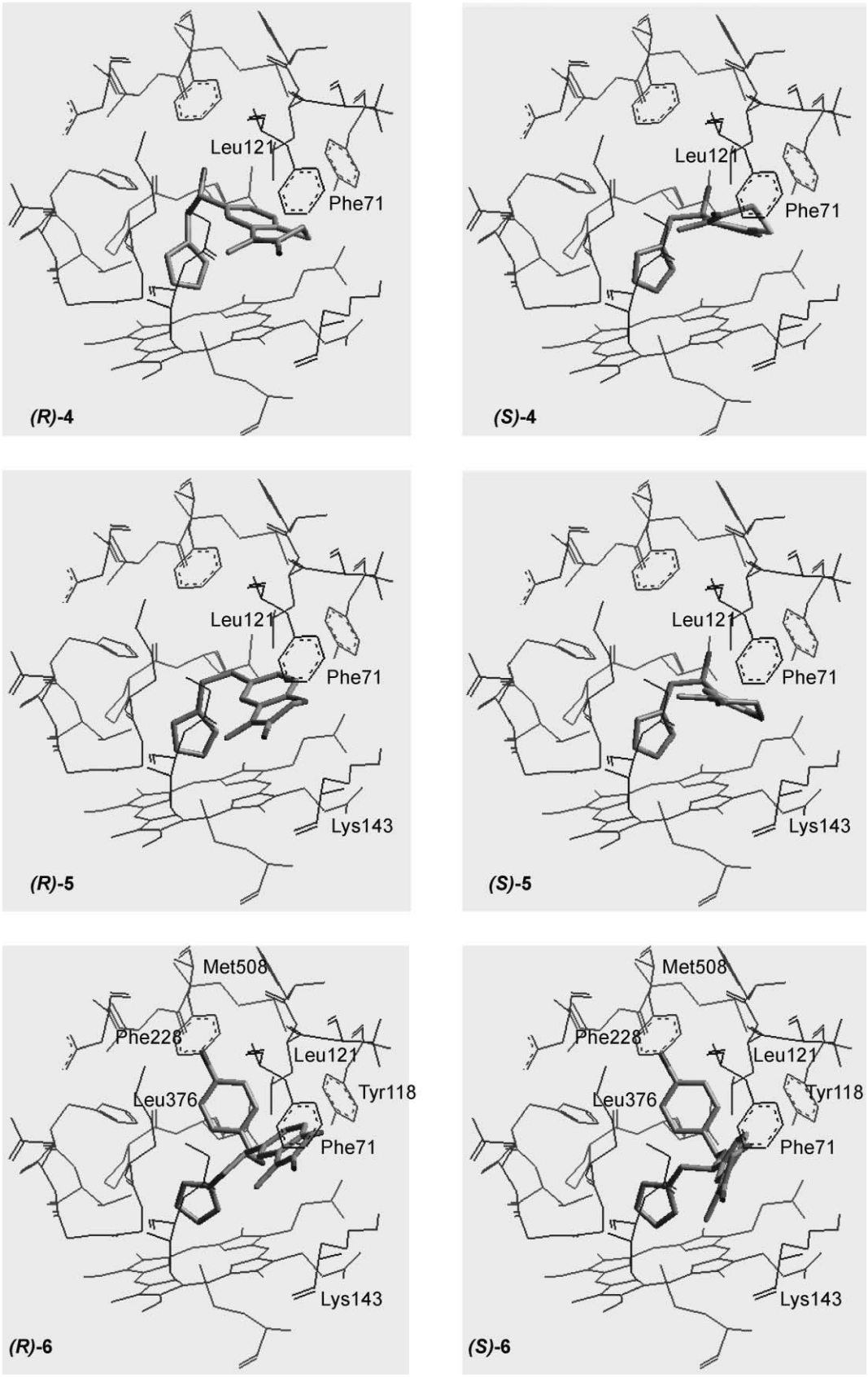

Figure 6. Docking solutions of the isomers of compounds **4**–**6** into the catalytic site of CA-CYP51.

Table 1. In vitro activity (MIC), energy of binding and logP values (AlogP) of studied compounds

Code name	MIC (μg/mL)	E_{bin} (kcal/mol)	AlogP
Fluconazole	1	−29.103	1.58
(*R*)-**1**	62.5	−19.100	3.07
(*S*)-**1**	62.5	−31.804	3.07
(*R*)-**2**	46	−15.510	3.07
(*S*)-**2**	46	−40.142	3.07
(*R*)-**3**	>250	−37.763	0.50
(*S*)-**3**	>250	−35.402	0.50
(*R*)-**4**	62.5	−26.532	0.50
(*S*)-**4**	62.5	−30.953	0.50
(*R*)-**5**	>250	−27.642	0.16
(*S*)-**5**	>250	−32.510	0.16
(*R*)-**6**	15.6	−16.882	2.73
(*S*)-**6**	15.6	−30.813	2.73

the side chain to position 7 of the benzothiazine nucleus and the free hydroxyl group, favor the binding of the *R* isomer over the *S*. Since both isomers adopt a similar binding mode, the subtle improvement in the binding energy of the *R* isomer is likely due to a better conformational strain energy of (*R*)-**3** (E_{conf} = 2.630 kcal/mol) compared to (*S*)-**3** (E_{conf} = 5.127 kcal/mol).

Methods

The sequences of cytochrome P450 14α-sterol demethylases of *M. tuberculosis* (MT-CYP51) and of *C. albicans* (CA-CYP51) were aligned using the Align123 module of Insight-II.[12] The Blosum-62 matrix was used with a gap penalty of 11 and a gap extension penalty of 1. Secondary structures were predicted using the PHD server.[13] The alignment was carefully checked to avoid gap insertion where conserved secondary structure motifs were present. Modeler module of Insight-II was used with the default setting to build a 3D model of CA-CYP51. The recently disclosed crystal structures of MT-CYP51 in complex with azole inhibitors (pdb codes: 1ea1; 1e9x) were used as templates. The atomic coordinates of the 3D model thus obtained were submitted to a minimization protocol using the Charmm22 force-field as implemented in Insight-II. During the minimization, a harmonic restraint of 20 kcal/(mol Å^2) was applied on the atomic coordinates of Cα atoms, whereas 400 kcal/mol was applied on the coordinates of the atoms belonging to the aromatic plane of the heme group. The energy minimization was performed using a cycle of 500 steps of Steepest Descendent algorithm followed by several cycles of Conjugate Gradient algorithm until a gradient of 0.01 kcal/mol was reached. A geometric validation of the structure was carried out by using the Procheck server[14] and Verify3D algorithm.[15] Where present, bad geometries were manually corrected and the structure minimized again with the above protocol.

Azole inhibitors were built using the sketch module of Cerius-2.[16] Each compound was minimized using the Universal force-field v.1.2[17] and the Smart Minimizer protocol of the Open Force Field module (OFF). Atomic charges were calculated using the semi-empirical Mopac/AM1 method.

Docking experiments were performed using a knowledge-based strategy.[18] Triazole antifungals bind to MT-CYP51 through the coordination of the nitrogen in position 4 of their azole rings to the sixth coordination position of the iron atom of the heme group. Accordingly, all compounds were manually docked by placing the nitrogen in position 3 of the imidazole ring at 2.37 Å from the heme iron on the center orthogonal of the heme plane in CA-CYP51. The above value is the average distance of Fe-N coordination bonds observed in crystallized complexes of MT-CYP51 with fluconazole and 4-phenylimidazole. Starting from this disposition, a reduced conformational profile of compounds was explored using a random sampling protocol as implemented in the Cerius-2 software package. Briefly, all torsional angles of azole inhibitors, except the Fe-N coordination bond, were varied randomly in a window of ±5° generating a number of 1000 conformations. For each enzyme/inhibitor complex the resulting conformers were clustered on the basis of the RMSD using the autocluster protocol implemented in the conformer analysis module of Cerius-2. The nuclei of each cluster, representing a docking solution, was submitted to a geometry optimization protocol. During the minimization, the protein was treated as a rigid body by applying fixed constraints on the coordinates of its atoms. Although this is a crude approximation, the rigid body treatment of the protein permits shifting of Charmm22 to OFF force-field without loosing the validated geometry of the protein. Moreover, the conformational strains induced in the inhibitors by the enzyme can be used as a qualitative index of the inhibitor's fit into the binding site. Energy minimization was performed using the Universal force-field v.1.2 and the Smart Minimizer protocol of the OFF module implemented in Cerius-2. In particular, the high convergence option was used to stop the minimization cycles. The value of the dielectric constant of the protein surrounding the binding site of the heme group was reported to be 6.5,[19] thus a value of 6.5 was used for this parameter during all minimizations.

The conformational strain energy cost of the inhibitors to reach the bioactive conformation from the global minimum was determined using a dielectric constant of 80 according to the hypothesis that this process occurs in the water. The refined docking solutions were ranked according to their binding energy. For each enzyme/inhibitor complex, only the best solution in terms of binding energy was stored and used for further analysis. The binding energies were calculated using the following equation:

$$E_{bin} = E_{int} + E_{conf} \quad (1)$$

Where the energy of binding (E_{bin}) is obtained from the sum of the interaction energy (E_{int}) and the conformational strain energy (E_{conf}). The interaction energy (E_{int}) is calculated with eq 2 from the docking solutions of each compound.

$$E_{int} = E_{complex} - (E_{compound} + E_{protein}) \quad (2)$$

Here, $E_{complex}$ is the energy of the complex, $E_{compound}$ is the energy of the docked compound, and $E_{protein}$ is the energy of the enzyme.

The conformational strain energy (E_{conf}) is calculated as the difference between the energy of the docked conformation and the energy of the global minimum for each compound (eq 3).

$$E_{conf} = E_{compound} - E_{global} \quad (3)$$

All calculations were carried out on SGI O2 R5000 and R10000 workstations.

Conclusion

A 3D model of the cytochrome P450 14α-sterol demethylase of *C. albicans* (CA-CYP51) was built on the basis of the sequence homology with the recently reported crystal structure of the cytochrome P450 14α-sterol demethylases of *M. tuberculosis* (MT-CYP51). The model of CA-CYP51 was exploited to explain the antifungal activity of a set of 1,4-benzothiazine and 1,4-benzoxazine imidazole derivatives. All compounds adopt similar binding modes inside the catalytic site of CA-CYP51. However, subtle differences of interactions and logP values, affect the in vitro antifungal activity of these compounds. These results will be used to address the design and synthesis of new potent antifungal compounds endowed with anti-*Candida* activity.

References and Notes

1. Imwidthaya, P.; Poungvarin, N. *Postgrad. Med. J.* **2000**, *76*, 85.
2. Steenbergen, J. N.; Casadevall, A. *J. Clin. Microbiol.* **2000**, *38*, 1974.
3. Maertens, J. A.; Boogaerts, M. A. *Curr. Pharm. Des.* **2000**, *6*, 225.
4. Sheehan, D. J.; Hitchcock, C. A.; Sibley, C. M. *Clin. Microbiol. Rev.* **1999**, *12*, 40.
5. Lamb, D.; Kelly, D.; Kelly, S. *Drug Res. Updates* **1999**, *2*, 390.
6. Fringuelli, R.; Schiaffella, F.; Bistoni, F.; Pitzurra, L.; Vecchiarelli, A. *Bioorg. Med. Chem.* **1998**, *6*, 103.
7. Pitzurra, L.; Fringuelli, R.; Perito, S.; Schiaffella, F.; Barluzzi, R.; Bistoni, F.; Vecchiarelli, A. *Antimicrob. Agents Chemother.* **1999**, *43*, 2170.
8. Schiaffella, F.; Guarraci, A.; Fringuelli, R.; Pitzurra, L.; Bistoni, F.; Vecchiarelli, A. *Med. Chem. Res.* **1999**, *9*, 291.
9. Fringuelli, R.; Pietrella, D.; Schiaffella, F.; Guarraci, A.; Perito, S.; Bistoni, F.; Vecchiarelli, A. *Bioorg. Med. Chem.* **2002**, *10*, 1681.
10. Podust, L. M.; Poulos, T. L.; Waterman, M. R. *PNAS* **2001**, *98*, 3068.
11. Ghose, A. K.; Viswanadhan, V. N.; Wendoloski, J. J. *J. Phys. Chem.* **1998**, *102*, 3762.
12. *Insight-II*; Accelrys: San Diego, CA.
13. The Predict Protein Server at URL: http://cubic.bioc.columbia.edu/predictprotein/
14. (a) Laskowski, R. A.; MacArthur, M. W.; Moss, D. S.; Thornton, J. M. *J. Appl. Cryst.* **1993**, *26*, 283. (b) Morris, A. L.; MacArthur, M. W.; Hutchinson, E. G.; Thornton, J. M. *Proteins* **1992**, *12*, 345 (URL: www.biochem.ucl.ac.uk/~roman/procheck/procheck.html.).
15. Luthy, R.; Bowie, J. U.; Eisenberg, D. *Nature* **1992**, *356*, 83.
16. Cerius-2, Accelrys, San Diego, CA.
17. Rappe, A. K.; Casewit, C. J.; Colwell, K. S.; Goddard, W. A.; Skiff, W. M. *J. Am. Chem. Soc.* **1992**, *114*, 10024.
18. Ji, H.; Zhang, W.; Zhou, Y.; Zhang, M.; Zhu, J.; Song, Y.; Lü, J.; Zhu, J. *J. Med. Chem.* **2000**, *43*, 2493.
19. Chimoni, E.; Tsfadia, Y.; Nachliel, E.; Gutman, M. *Biophys. J.* **1993**, *64*, 472.